Structure and phase transition in pyridazine perchlorate

2007 J. Phys.: Condens. Matter 19 086219

(http://iopscience.iop.org/0953-8984/19/8/086219)

IOP PUBLISHING JOURNAL OF PHYSICS: CONDENSED MATTER

J. Phys.: Condens. Matter **19** (2007) 086219 (12pp) doi:10.1088/0953-8984/19/8/086219

Structure and phase transition in pyridazine perchlorate

B Kosturek[1], A Waśkowska[2], S Dacko[1] and Z Czapla[1]

[1] Institute of Experimental Physics, University of Wrocław, M Borna 9, 50-204 Wrocław, Poland
[2] Institute of Low Temperature and Structure Research, Polish Academy of Sciences, Okólna 2, 50-422 Wrocław, Poland

Received 17 May 2006, in final form 28 November 2006
Published 9 February 2007
Online at stacks.iop.org/JPhysCM/19/086219

Abstract

Single crystals of pyridazine perchlorate $[(C_4H_4N_2)HClO_4]$ have been synthesized and characterized by x-ray diffraction, dielectric measurements and optical studies. At room temperature the crystal is monoclinic, space group $P2_1/n$. The temperature dependences of the electric permittivity and birefringence exhibit anomalous behaviour, characteristic of the first-order phase transitions at 343 and 339 K on heating and cooling, respectively. Optical investigations under a polarizing microscope show that the crystal symmetry changes from the biaxial room temperature phase II to the optically uniaxial high temperature phase I. The domain pattern arising after cooling from phase I reflects observed symmetry changes at phase transition. The fully disordered structure of phase I can be described in the obverse hexagonal space group $R\bar{3}m$.

1. Introduction

Organic–inorganic crystals containing pyridinium or imidazolium cations and AX_4 anions, where A = B, Cl, I and X = F, O, exhibit diverse phase transitions of a structural and ferroic nature. Their properties have been the subject of numerous studies [1–6]. The molecular mechanism of the phase transitions in this class of compounds is related to the dynamics of constituent cationic and anionic units. Synthesis of pyridazine salt $[(C_4H_4N_2)HClO_4]$ was undertaken in the search for new ferroic materials based on planar cationic units, which can potentially be involved in the formation of hydrogen bonds. The aim of the present paper is to describe the single crystal growth and the results of studies on the structure and temperature dependent properties of the compound investigated by using an x-ray diffraction technique, dielectric and linear birefringence measurements as well as an optical analysis of the domain structure under a polarizing microscope.

2. Experimental details

Polycrystals of pyridazine perchlorate were obtained from stoichiometric quantities of pyridazine and perchloric acid. Single crystals were grown from a saturated water solution at a

Table 1. Crystal data and structure refinement for pyridazine perchlorate $C_4H_4N_2HClO_4$ at room temperature and 350 K.

Crystal data	Phase II	Phase I
Temperature (K)	293(2)	350
Crystal system,	Monoclinic	Hexagonal
Space group	$P2_1/n$,	$R\bar{3}m$
Unit cell dimensions (Å)	$a = 5.2820(11)$	8.697 (1)
	$b = 8.6790(17)$	8.697(1)
	$c = 15.039(3)$	8.350(2)
	$\beta = 94.98(3)^\circ$	$\gamma = 120^\circ$
Volume (Å^3)	686.8(2)	546.96(3)
Z, calculated density (Mg m^{-3})	4, 1.746	3, 1.644
Absorption coefficient (mm^{-1})	0.522	0.499
Crystal size (mm)	$0.35 \times 0.31 \times 0.28$	$0.4 \times 0.35 \times 0.3$
Data collection		
Wavelength (Å)	0.71073	
θ range for data collection (deg)	3.59–45.78	4.5–27.9
Limiting indices: h:	−8, 10	−10, 11
k:	−17, 11	−11, 11
l:	−25, 24	−10, 10
Reflections collected/unique	145161/4637	5590/1827
Reflections $>2\sigma(I)$	1732	174
Refinement method	Full-matrix least-squares on F^2	
Data/restraints/parameters	1732/0/105	174/0/14
R_{int} before, after abs. correction	0.082, 0.037	0.052, 0.031
Refinement		
Goodness-of-fit on F^2	1.038	1.075
Final R indices $[I > 2\sigma(I)]$	$R_1 = 0.037$,	0.081
	$wR_2 = 0.083$	0.203
Extinction coefficient	0.096(4)	0
Largest diff. peak and hole (e Å^{-3})	0.35; −0.43	0.036; −0.14

constant temperature of 303 K. A sample of dimensions given in table 1 was chosen for x-ray diffraction measurements on a single crystal *Xcalibur* diffractometer (Oxford Diffraction/CCD) with graphite monochromated Mo Kα radiation. The intensity data were collected using the ω-scan technique in steps of $\Delta\omega = 1.2$. The exposure time was 28 s per image. The 1150 images taken in nine sets of exposures at different angular positions covered about 98% of the Ewald sphere. Crystal and the instrument stability was controlled by one image, selected as a standard and measured after every 50 images. The intensities, corrected for Lorentz and polarization effects, were integrated and numerical absorption correction based on the crystal shape was applied [7]. The structure was solved with direct methods and refined by a full matrix least-squares method on F^2 data (SHELXS97 and SHELXL97 program systems, respectively [8, 9]). Hydrogen atoms were included from geometry and constrained at their positions assuming a 'ride-on' model with refined isotropic temperature factors except for the H(2) atom, which was fixed at the calculated position. High temperature data were collected at 350 K for the crystal heated with a Kuma Diffraction temperature controller. As the scattering power of the crystal at this temperature was much poorer and reflections with intensities $I > 2\sigma$ were observed in the 2θ range limited to 56°, the exposure time was prolonged to 35 s/image. Crystal

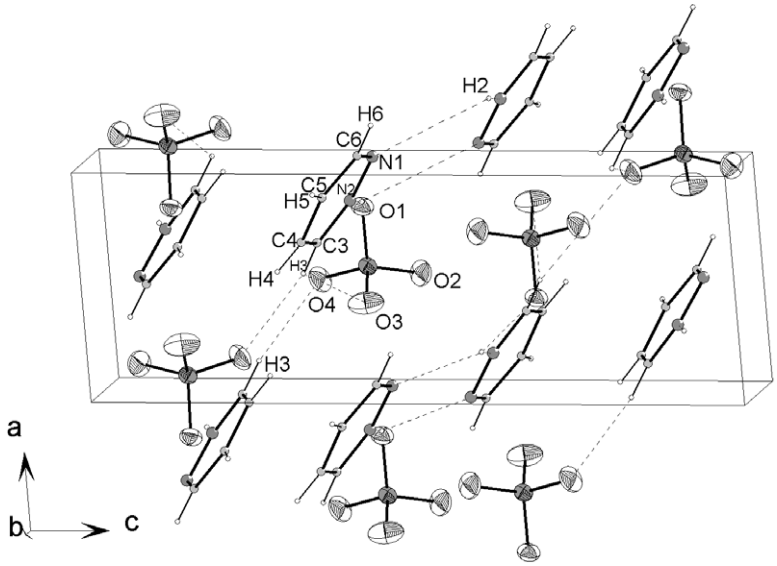

Figure 1. Projection in the *b*-axis of the pyridazine perchlorate structure at room temperature.

data and further experimental details are summarized in table 1 together with the refinement parameters.

Dielectric measurements were carried out on platelets about 0.5 mm thick, cut out from a large crystal with the faces perpendicular to the a, b, c^* and $[\bar{1}01]$ crystallographic directions. Silver paste was used as the electrodes. The capacity of the samples was measured using a HP 4284A precision LCR meter in the frequency range 1 kHz–1 MHz. The amplitude of measuring field was 4 V cm^{-1}. The measurements were performed in heating/cooling runs at a rate of 0.3 K min^{-1}. Thermal hysteresis and kinetics were controlled by additional measurements at a rate of 0.15 K min^{-1}. Optical studies were carried out under a Polam 113 polarizing microscope. Changes in linear birefringence were measured with a rotating-analyser method [10] with a 1 mW He–Ne laser ($\lambda = 632.8$ nm) as a light source. The absolute value of the linear birefringence (LB) at room temperature and the amplitude of the LB jump at the phase transition were determined by using an Ehringhaus compensator ensuring an accuracy of 5%. These data were obtained from samples with faces perpendicular to the b and $[\bar{1}01]$ directions of the room temperature unit cell. The temperature dependent measurements of LB were done at a rate of 0.5 K min^{-1} in the range 300–355 K and with 0.2 K min^{-1} in the phase transition region. Nucleation and dynamics of the phase front were observed in the quasistatic regime with a rate below 0.1 K min^{-1}.

Additional DSC measurements were carried out using a Perkin-Elmer TMA-7 calorimeter with rates ranging from 5 to 20 K min^{-1}.

3. Results and discussion

3.1. Crystals and x-ray structure at room temperature

Good quality large crystals were obtained after about 20 days of continuous growth. Their habit suggested monoclinic symmetry. The crystals exhibit a cleavage in the crystallographic (001) plane. The crystal structure of phase II with the atom numbering scheme is shown in figure 1.

Table 2. Atomic coordinates ($\times 10^4$) and equivalent isotropic displacement parameters (Å^2 $\times$ 10^3) for $C_4H_5N_2ClO_4$ at room temperature. U(eq) is defined as one-third of the trace of the orthogonalized Uij tensor.

	x	y	z	U(eq)
Cl(1)	916(1)	7319(1)	1392(1)	32(1)
O(1)	−1735(1)	7716(1)	1378(1)	47(1)
O(2)	1307(2)	400(1)	628(1)	66(1)
O(3)	2393(2)	8686(1)	1407(1)	76(1)
O(4)	1605(2)	6423(1)	2176(1)	67(1)
N(1)	4592(2)	1570(1)	530(1)	40(1)
N(2)	6591(2)	884(1)	951(1)	40(1)
C(3)	8365(2)	1556(1)	1488(1)	39(1)
C(4)	8175(2)	3128(1)	1656(1)	38(1)
C(5)	6139(2)	3892(1)	1251(1)	39(1)
C(6)	4391(2)	3066(1)	692(1)	39(1)

Table 2a. Anisotropic displacement parameters (Å^2 $\times$ 10^3) for $C_4H_5N_2ClO_4$ at room temperature. The anisotropic displacement factor exponent takes the form: $-2\pi^2[h^2\mathbf{a}^{*2}U11 + \cdots + 2hk\mathbf{a}^*\mathbf{b}^*U12]$.

	$U11$	$U22$	$U33$	$U23$	$U13$	$U12$
Cl(1)	32(1)	29(1)	36(1)	−1(1)	−1(1)	3(1)
O(1)	34(1)	51(1)	55(1)	2(1)	−2(1)	10(1)
O(2)	75(1)	72(1)	52(1)	−22(1)	7(1)	18(1)
O(3)	57(1)	42(1)	131(1)	−5(1)	17(1)	−15(1)
O(4)	68(1)	79(1)	50(1)	17(1)	−12(1)	19(1)
N(1)	40(1)	36(1)	43(1)	1(1)	−12(1)	−2(1)
N(2)	44(1)	26(1)	48(1)	−2(1)	−5(1)	2(1)
C(3)	35(1)	39(1)	41(1)	1(1)	−4(1)	4(1)
C(4)	39(1)	40(1)	35(1)	−6(1)	−2(1)	−8(1)
C(5)	46(1)	29(1)	41(1)	−2(1)	7(1)	2(1)
C(6)	36(1)	37(1)	42(1)	6(1)	−2(1)	4(1)

The atomic positions and their isotropic thermal displacement amplitudes, U(eq), are given in table 2. The analysis of anisotropic displacements shows that there is no structural disorder resulting from enhanced thermal movement (table 2a).

The formula unit consists of a monoprotonated, flat pyridazine unit $[C_4H_5N_2]^+$ and a slightly distorted tetrahedral ClO_4^- group. Selected interatomic bond distances and angles in the molecule are listed in table 3. The protonation taking place at N(2) leads to the formation of the bifurcated hydrogen bond system (HB) involving the H(2) atom. One of these bonds, N(2)–H(2)$\cdots$N(1)$_{1-x,-y,z}$ with N(1) and N(2) acting as an electron donor and acceptor, respectively, links two symmetry related pyridazine rings (figure 1). The second bond, N(2)–H(2)$\cdots$O(1)$_{x+1,y-1,z}$ forms interionic contacts with the ClO_4^- anion, causing elongation of the Cl–O(1) distance in the tetrahedron. Besides, two other HB interactions of the type C–H$\cdots$O are forming links between the cationic and anionic groups (figure 1).

Their geometry is given in table 4. Although HB in this structure can be considered as weak hydrogen bonds [11–17], a direct consequence of their presence is distortion of the ions, mainly of the tetrahedra (table 3). On the other hand the HB system stabilizes the structure in the sense that dynamical disorder, related to the thermally activated movements of the ions, is not observed at room temperature.

Table 3. Selected bond lengths (Å) and angles (deg) for pyridazine perchlorate at room temperature.

Cl(1)–O(3)	1.4188(8)
Cl(1)–O(4)	1.4280(9)
Cl(1)–O(2)	1.4326(8)
Cl(1)–O(1)	1.4405(9)
N(1)–N(2)	1.3239(11)
N(1)–C(6)	1.3267(13)
N(2)–C(3)	1.3186(13)
C(3)–C(4)	1.3931(16)
C(4)–C(5)	1.3612(14)
C(5)–C(6)	1.3836(17)
O(3)–Cl(1)–O(4)	109.43(5)
O(3)–Cl(1)–O(2)	111.23(7)
O(4)–Cl(1)–O(2)	108.33(6)
O(3)–Cl(1)–O(1)	109.43(5)
O(4)–Cl(1)–O(1)	108.60(6)
O(2)–Cl(1)–O(1)	109.26(5)
N(2)–N(1)–C(6)	115.15(8)
C(3)–N(2)–N(1)	125.09(8)
N(2)–C(3)–C(4)	119.0(1)
C(5)–C(4)–C(3)	117.5(1)
C(4)–C(5)–C(6)	118.4(1)
N(1)–C(6)–C(5)	123.75(9)

Table 4. Geometry of proposed hydrogen bonds (shortened intermolecular distances).

D–H$\cdots$A	d(D − H)	d(H$\cdots$A)	d(D$\cdots$A)	<(DHA)
N(2)–H(2)$\cdots$N(1)$_{1-x,-y,-z}$	0.915	2.436(4)	3.106(6)	142(4)
N(2)–H(2)$\cdots$O(1)$_{x+1,y-1,z}$	0.915	2.164(3)	2.943(4)	130(3)
C(3)–H(3)$\cdots$O(4)$_{3/2-x,y-1/2,1/2-z}$	0.980	2.405(5)	3.191(5)	136(4)
C(3)–H(3)$\cdots$O(3)$_{x+1,y-1,z}$	0.915	2.486(6)	3.285(5)	138(4)

3.2. High temperature structure at 350 K

Already at room temperature the structural motif and the ratio of $c/b = \sqrt{3} = 1.732$ display pseudo-hexagonal features (figure 2). Therefore the first approach to structural characterization in phase I was performed in the space group $P6_3/m$, being a supergroup of $P2_1/n$. This attempt, however, was unsuccessful because the multiplicity of allowed Wyckoff positions led to the number of formula units in the cell, $Z = 2$ or 4, being inconsistent with $Z = 3$ resulting from the cell volume in phase I, crystal density and molar volume. It was thus reasonable to adopt hexagonal symmetry for phase I with the unit cell given in table 1. The rhombohedral P-lattice with $a = b = c = 5.741$ Å and $\alpha = \beta = \gamma = 98.49°$, can be obtained using the transformation matrix (2/3, 1/3, 1/3; −1/3, 1/3, 1/3; −1/3 2/3 1/3). This structure has been described with the dynamical disorder model in space group $R\bar{3}m$. The hydrogen bonds present in phase II apparently became broken at 350 K. As a result of thermal activation, both the $(C_4H_4N_2)^+$ and ClO_4^- ions appeared to be fully disordered. In particular, the ring atoms are hoping among several local potential minima, and consequently the C and N atoms are able to occupy up to six equivalent positions of the 18 f site, with an average C–C distance 1.326(6) Å and bond angle of 120°. In this way the C and N atoms cannot be distinguished. Similarly the movements of the ClO_4 tetrahedron lead to pseudo-octahedral local symmetry

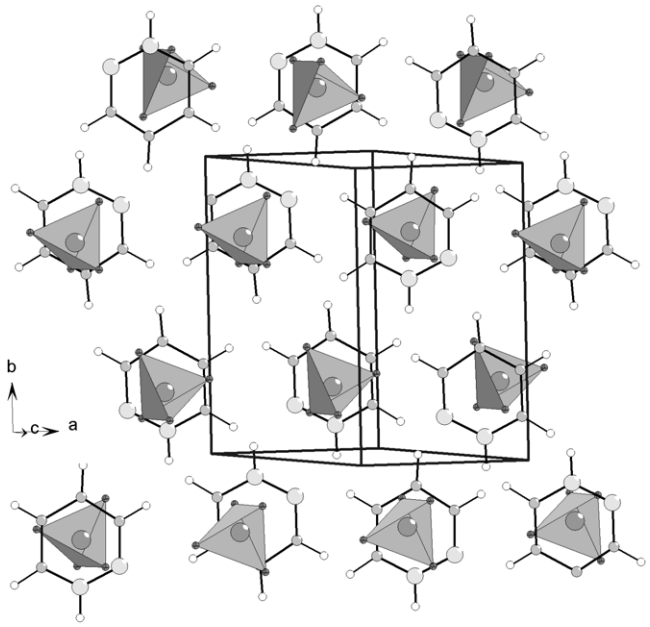

Figure 2. Pseudo-hexagonal arrangement of the structural units in $(C_4H_4N_2)HClO_4$ in phase II.

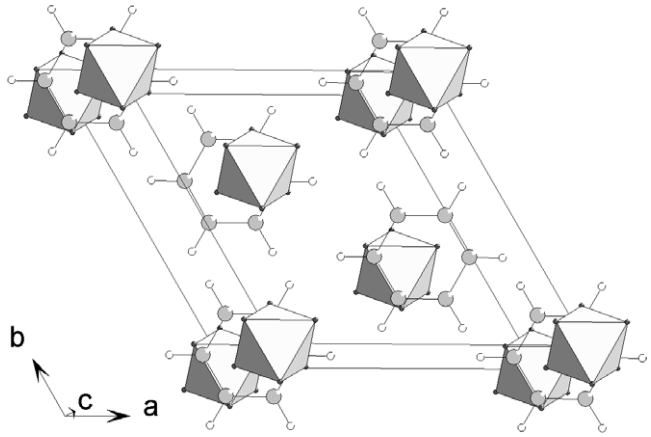

Figure 3. High temperature phase I of $(C_4H_4N_2)HClO_4$ depicted in the hexagonal cell ($R\bar{3}m$).

around the central Cl, with a Cl–O distance of 1.419(9) Å. In the present model (figure 3) the site symmetry corresponds to the average of the dynamic positions of the ions, suggesting that the real crystal symmetry might be lower than that found. The above model corresponds well with obtained reproducible DSC data on phase transition heat -12 kJ mol^{-1} and transition entropy -35 J mol^{-1} K^{-1}.

However, careful examination of the Ewald sphere and intensity data did not show any superstructure reflections. In addition, it was impossible to obtain by Fourier synthesis a consistent model for other symmetries. Therefore, we propose the structure of phase I with fully disordered ions. The atomic positional parameters are given in table 5.

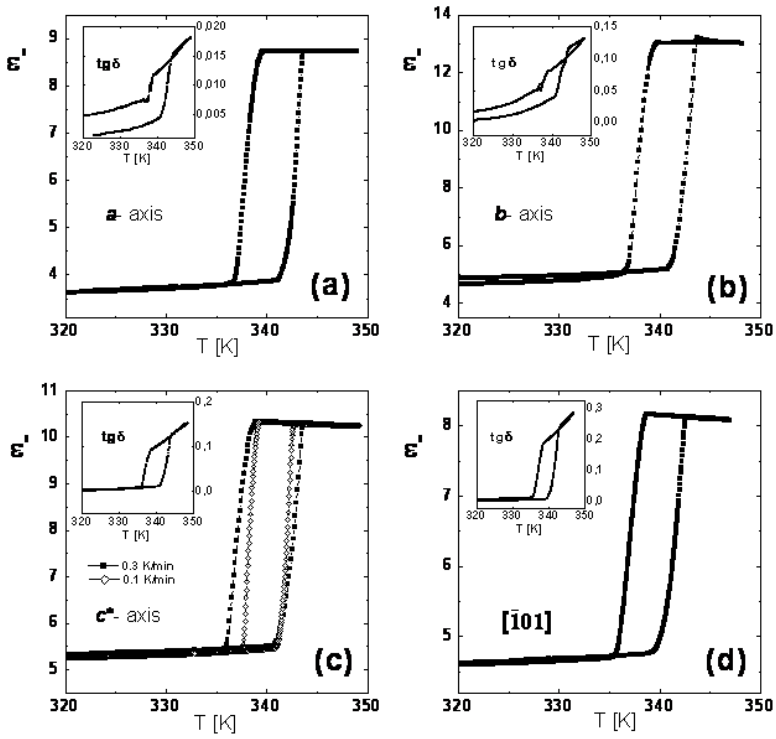

Figure 4. Dielectric permittivity and losses (insets) measured at a frequency 10 kHz along the *a*-, *b*-, c^*- and [$\bar{1}$01] crystallographic directions of phase II.

Table 5. Atomic coordinates ($\times 10^4$) and anisotropic displacement parameters (Å^2 $\times$ 10^3) for $C_4H_5N_2ClO_4$ at 350 K. The anisotropic displacement factor exponent takes the form: $-2\pi^2[h^2\mathbf{a}^{*2}U11 + \cdots + 2hk\mathbf{a}^*\mathbf{b}^*U12]$.

Atom	Site	x	y	z	$U11$	$U22$	$U33$	$U23$	$U13$	$U12$
Cl	3a	0.0	0.0	0.0	108(2)	108(2)	108(2)	0.0	0.0	54.1(1)
O(1)	18h	−765(7)	765(7)	981(14)	224(9)	224(9)	254(11)	−36(4)	39(4)	137(9)
C(1)	18f	−1808(2)	3333(0)	−1667(0)	88(3)	124(4)	154(5)	−4(3)	−2(5)	62(2)
H(1)	18f	−739(2)	3333(0)	−1667(0)	141(12)					

3.3. Dielectric properties

The results of dielectric measurements are presented in figure 4. The value of permittivity at room temperature appears to be rather small in all crystal directions. On the heating run, at about 341 K, the anomalous increase of permittivity starts and it ends at 343 K. Beyond this temperature range the changes are insignificant.

In the same temperature range an increase in $\tan\delta$, especially at lower frequencies, is observed. Similar effects are also seen on cooling. Such an anomalous evolution of permittivity and $\tan\delta$ evidences the first-order nature of the phase transition. The thermal hysteresis of the transition is about 3 K. The increase in permittivity is indicative of reorientational freedom of dipolar units, which appear in the crystal lattice above the transition. An increase in $\tan\delta$ is most probably related to the ionic conductivity. Thus, the present observations lead to the conclusion that above 343 K the ordered room temperature phase transforms to the disordered

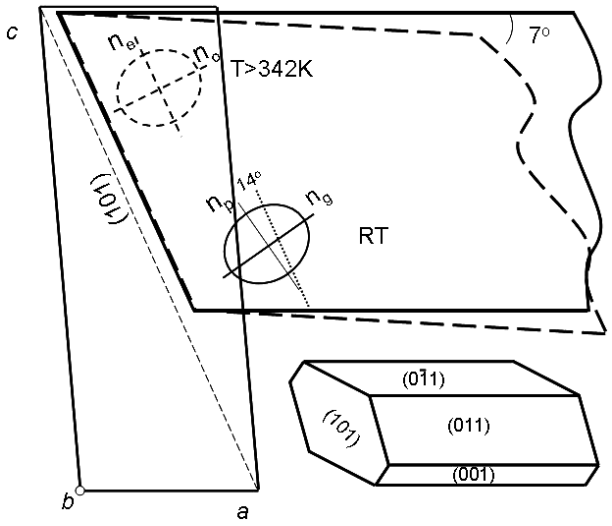

Figure 5. The crystal shape and orientation of the optical indicatrix in phases I and II viewed along the *b*-axis of the room temperature phase. The optically uniaxial phase I is denoted with dashed lines.

one. For further information on the nature of the transition, an additional heating/cooling cycle has been performed at a the rate of 0.15 K min^{-1} and the result is shown in figure 4(c). It can be noticed that the permittivity variations are limited to a range of about 1.0 K, in comparison with 2 K observed on heating/cooling at a rate of 0.3 K min^{-1}. However, the thermal hysteresis remained practically the same. We thus conclude that the phase transition proceeds slowly and the kinetics of the transition is its specific feature. The electric permittivity was additionally measured in the [$\bar{1}$01] direction appearing to be the unique axis of the high temperature phase because, as will be shown below in our optical studies, the phase transformation is most probably between the monoclinic and rhombohedral phases. The result shown in figure 4(d) is similar to those from the measurements in directions of the crystallographic axes of the room temperature phase. It is worth noting that the permittivity measured on cooling, when approaching room temperature from above, has practically the same value as in the low temperature phase before heating. Thus, based on the dielectric studies it can be stated that pyridazine perchlorate exists in two phases—phase I above 343 K (on heating) and phase II below 336 K (on cooling).

3.4. Optical studies

Optical observations were first done on the *b*-cut sample. As-grown crystals are optically homogeneous and no ferroelastic domains have been observed. The shape of the crystal and projection of the unit cell at room temperature together with the positions of the optical indicatrix in relation to the crystallographic axes in the *ac* plane of phase II and in the high temperature phase I (dashed line) are illustrated in figure 5.

Relative to the orientation of the indicatrix in the room temperature phase, the main axes of indicatrix in phase I are turned by about 14° in such a way that the [$\bar{1}$01] direction of phase II corresponds to the unique axis of the optical indicatrix in phase I. This rotation is coupled with the crystal deformation as shown schematically in figure 5. The birefringence values in the room temperature phase II are equal to $\Delta n_{\mathrm{m}} = 0.19$, $\Delta n_{\mathrm{g}} = 0.17$, $\Delta n_{\mathrm{p}} = 0.02$.

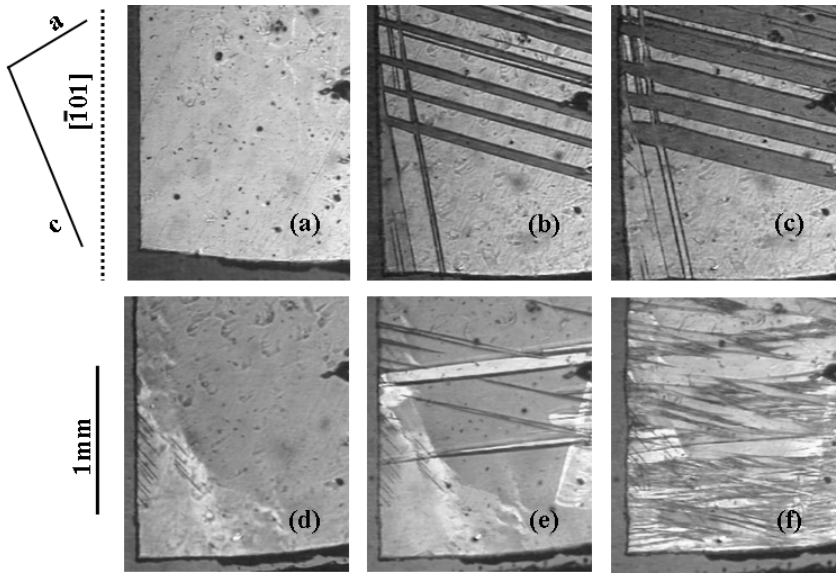

Figure 6. The *b*-plate of the pyridazine perchlorate crystal in polarized light: (a) virgin crystal at room temperature; (b) and (c) the stripes of phase I on heating from phase II; (d) crystal surface in phase I ($T > 343$ K); (e) the stripes of phase II on cooling from phase I ($T \sim 338$ K); (f) domain pattern at room temperature.

Nucleation of the new phase front is illustrated in figure 6. The first heating run reveals the appearance and growth of the high temperature phase (I) in the form of two kinds of stripe with the interfaces inclined to the a-axis by 69° and 42°. On further heating the stripes of the new phase continue to grow slowly. In the quasi-static temperature regime the appearance of the new phase takes a few minutes and its development can be held since the two phases are in equilibrium.

In phase I, the angle between the crystal edge nearly normal to the monoclinic (101) plane and the natural (101) crystal face decreases by about 7° (figures 6(a) and (d)). Besides, the natural edges of the crystal become deformed after cooling to the room temperature phase (figure 6(f)). After transition to phase I the studied samples are optically homogeneous. However, at the meeting places of the stripes with different orientations the crystal becomes stressed, probably due to a concentration of dislocations resulting from interaction between different interfaces [18] (figures 6(d), (e), the areas with lowered extinction). Optical observation on the cooling run showed the appearance of phase II at about 338 K (figure 6(e)) and a domain-like mosaic structure at room temperature (figure 6(f)). The mosaic domain structure disappears after heating above the phase transition temperature. Subsequent cooling leads to practically the same mosaic structure, characteristic of phase II. To try and determine the possible symmetry of phase I, a sample cut perpendicular to the [$\bar{1}$01] crystallographic direction was prepared. This direction is close to the acute bisectrix of the optical axes in phase II and parallel to the unique axis of the indicatrix in phase I. During heating above the phase transition temperature it turned out that the conoscopic figures changed from biaxial to uniaxial. The position of the optical axis was shifted relative to the acute bisectrix by one-quarter of the angular distance between two optical axes of phase II. The monoclinic direction [$\bar{1}$01] thus becomes the direction of the unique axis in phase I.

A sample prepared in the same way as above was observed under a polarizing microscope on heating and cooling runs. On heating, domains of the new phase with the interfaces nearly

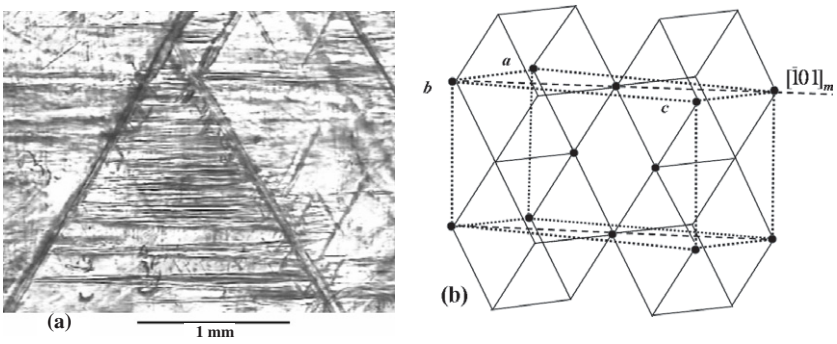

Figure 7. (a) Domain pattern observed in the $[\bar{1}01]$ direction of monoclinic pyridazine perchlorate after cooling from phase I; (b) proposed schematic relation between the monoclinic and hypothetical rhombohedral unit cell of phase I.

normal to the observation direction were seen and appeared as wide interference colour bands. When this sample was cooled from phase I to phase II, a more complex domain structure was observed—three domains groups with walls nearly parallel to the monoclinic $[\bar{1}01]$ direction turned by 60° (120°) to each other, as illustrated in figure 7(a).

It is clearly seen that the threefold (or sixfold) symmetry axis disappears at the phase transition. Taking into consideration the shape of the monoclinic unit cell comprising four formula units and pseudotrigonal packing of the molecules at room temperature (figure 7(b)) together with the observations described above, one can construct a model of the monoclinic cell built of two rhombohedral cells doubled along the rhombohedral [111] direction, as shown in figure 7(b). This allowed the suggestion that the symmetry of the new phase should be rhombohedral with the triad axis parallel to the monoclinic $[\bar{1}01]$ direction and a transition of antiferrodistortive character [18]. This was confirmed by the results of structural investigations of the high temperature phase I. So we cannot apply a simple symmetry analysis to the resulting domain pattern [18, 19].

During the growth process crystals with one orientation state in phase II were obtained. A change to another state would require a large energy to overcome the energetic barrier, and this is impossible at the growth temperature used. However, on cooling from phase I, all orientation states may appear with the same probability and therefore we can observe the domain structure reflecting changes in point symmetry at the transition between rhombohedral and monoclinic crystallographic systems. We were not able to change the domain pattern by applying mechanical stress even in the vicinity of the phase transition temperature as the observed domains are the result of different orientations of the nucleus of the new phase and its wall (or interface) orientation is defined by equal deformation of two phases, not two ferroelastic twins [19].

The linear birefringence measurements along the *b*- and $[\bar{1}01]$ directions, respectively, are shown in figure 8. Anomalous behaviour starts at 340 K and ends at 341 K, confirming the phase transition of the first order. The birefringence could not be measured properly on cooling below the transition at 337 K due to the domain structure. Consistent with the dielectric properties we can make a statement that the phase transition is reversible and strongly of order I. The results of measurements in the $[\bar{1}01]$ direction are close to the expected morphic birefringence changes at the transition from monoclinic to the optically uniaxial phase, where birefringence is practically equal to zero, despite a small disorientation resulting from the spontaneous strain.

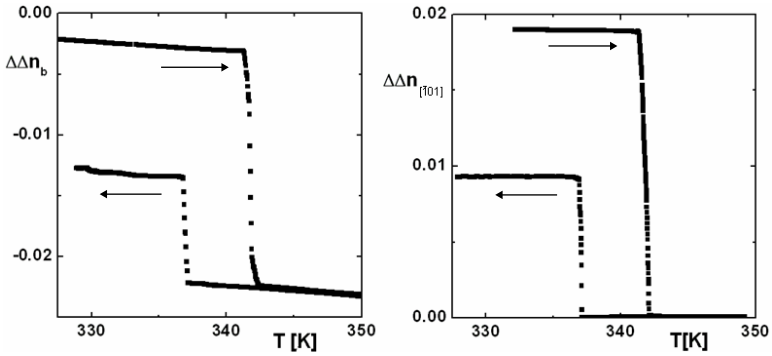

Figure 8. The temperature changes of the linear birefringence in the phase transition region.

4. Summary

The presented studies can be summarized as follows:

(1) X-ray diffraction data have shown that the room temperature structure of pyridazine perchlorate is monoclinic, $P2_1/n$. It is stabilized by a system of hydrogen bonds linking the distorted ClO_4^- anionic groups and flat rings of the protonated pyridazine. All atoms in the molecule are well located at their positions and thermal displacement amplitudes do not show any anomalous features. Thermally activated vibrations of the molecular units in the high temperature phase I caused the interionic hydrogen bonds to be broken, leading in consequence to the fully disordered structure modelled in the hexagonal space group $R\bar{3}m$, which is consistent with high values of the transition heat and entropy -12 kJ mol^{-1} and 35 J mol^{-1} K^{-1}.
(2) Dielectric and birefringence measurements evidenced structural phase transition of first order at $T = 343$ K with thermal hysteresis of about 3 K.
(3) Optical observations along the b-axis have shown the propagation of the phase front, characteristic of the first-order phase transition. In the region of the transition, a coexistence of the two phases was observed. The domain structure arriving on cooling to phase II disappeared after heating to phase I.
(4) The domain pattern observed along the $[\bar{1}01]$ direction and transformation to the optically uniaxial system reflects the hexagonal symmetry of phase I. Three orientations of the interface between trigonal and monoclinic symmetry have been observed on cooling.

Acknowledgments

This work was supported by the University of Wrocław under grant 2016/W/IFD/2006. We thank Professor Adam Pietraszko (ILT&SR) for his help in the collection of x-ray intensity data at 350 K.

References

[1] Czarnecki P, Nawrocik W, Pająk Z and Wąsicki J 1994 *Phys. Rev.* B **49** 1511
[2] Czarnecki P, Nawrocik W, Pająk Z and Wąsicki J 1994 *J. Phys.: Condens. Matter* **6** 4955
[3] Czapla Z, Dacko S and Kosturek B 2000 *Z. Naturf.* a **55** 891
[4] Pająk Z, Czarnecki P, Szafrańska B, Małuszyńska H and Fojud Z 2004 *Phys. Rev.* B **69** 132102
[5] Czapla Z, Dacko S, Kosturek B and Waśkowska A 2005 *Phys. Status Solidi* b **242** R122–4

[6] Eilerman D and Rudman R 1980 *J. Chem. Phys.* **72** 10
[7] Oxford Diffraction 2001 *CrysAlis CCD and CrysAlis RED* 9 Oxford Diffraction Ltd
[8] Sheldrick G M 1997 *SHELXS97, Program for Solution of Crystal Structures* University of Göttingen, Germany
[9] Sheldrick G M 1997 *SHELXl97, Program System for the Determination and Refinement of Crystal Structures* University of Göttingen, Germany
[10] Wood J G and Glazer A M 1979 *J. Appl. Crystallogr.* **13** 207
[11] Taylor R and Kennard O 1983 *Acta Crystallogr.* B **39** 133
[12] Berkovitch-Yellin L and Leiserowitz L 1984 *Acta Crystallogr.* B **40** 159
[13] Hernandez R P, Rodriguez J D, de Armas H N and Toscano R A 1996 *Acta Crystallogr.* C **52** 203
[14] Xu D and Zhang S 1999 *Chem. Phys. Lett.* **301** 449
[15] Xu D and Ratajczak H 2003 *Chem. Phys. Lett.* **371** 601
[16] Xu D and Ratajczak H 2005 *J. Mol. Struct. (Theochem)* **716** 207
[17] Xu D and Ratajczak H 2005 *J. Mol. Struct.* **716** 37
[18] Salje E K H 1990 *Phase Transformations in Ferroelastic and Co-Elastic Crystals* (Cambridge: University Press)
[19] Boulesteix C, Yangui B, Ben Salem M, Manolikas C and Amelinckx S 1986 *J. Physique* **47** 461